Stress evolution in sputter-deposited Fe–Pd shape-memory thin films

Y. Sugimura, I. Cohen-Karni, P. McCluskey, and J.J. Vlassak[a)]
Division of Engineering and Applied Sciences, Harvard University, Cambridge, Massachusetts 02138

(Received 1 October 2004; accepted 19 January 2005)

Fe–Pd films with Pd content varying between 26 and 30 at.% have been deposited by means of magnetron sputtering of elemental Fe and Pd targets. As-deposited films are highly supersaturated solid solutions of Pd in Fe that have a body-centered-cubic crystal structure and a very fine grain size. Substrate curvature measurements indicate that the films undergo an irreversible densification when heated above 100 °C. This densification is attributed to a structural change that is also observed in other supersaturated systems with a substantial atomic size difference between the constituents. It is possible to retain the high-temperature austenite phase at low temperature by annealing the films at 900 °C followed by rapid cooling. Depending on film composition, this metastable austenitic phase transforms to either a body-centered tetragonal (bct) or a face-centered tetragonal (fct) martensite around room temperature. Substrate curvature measurements show that formation of the fct martensite is reversible, while that of bct martensite is not. The fct transformation occurs at lower Pd content and higher temperature than reported for bulk materials. Both the fct and the fcc phase show a strong Invar effect at lower temperature and Pd content than observed in the bulk.

I. INTRODUCTION

Shape-memory alloys can recover large strains due to a thermoelastic martensitic transformation that takes place in these materials. They have been studied extensively over the last 50 years, and Ni–Ti alloys in particular have been developed successfully into actuators and sensors in various engineering applications. If the martensitic or austenitic phases are ferromagnetic, it is sometimes possible to control the martensitic transformation through application of a magnetic field. In some materials, for instance, the transformation can be induced by applying a strong enough magnetic field.[1] Alternately, a magnetic field can be used to convert martensitic variants or twins in the martensitic phase. Application of a magnetic field causes variants with their easy axis of magnetization aligned with the externally applied field to grow at the expense of others. The result is a macroscopic shape change. This magnetic shape memory effect is distinctly different from the well-known magnetostriction phenomenon in that the strain obtained in the magnetic shape memory is orders of magnitude larger than for magnetostriction.

A number of ferromagnetic materials have been studied in the past including the Fe–Ni, Fe–Pt, Fe–Pd, Co–Ni, Fe–Co–Ni–Ti systems in addition to intermetallics based on the Heusler-phase Ni_2MnGa. These studies[2–8] have shown that among these alloy systems, Ni_2MnGa, Fe–Pd, and ordered Fe_3Pt have the potential to be used as ferromagnetic shape-memory alloys. Thus far, only limited research[9–13] has been conducted on Fe–Pd thin films and their mechanical behavior remains largely unexplored.

At room temperature, the equilibrium phases in the Fe–Pd composition range of interest are the α-Fe phase and the ordered Fe–Pd phase. At elevated temperature, the face-centered cubic austenite phase is stable. It is possible, however, to retain the austenite phase at room temperature using an appropriate heat treatment. In bulk alloys with a Pd content of approximately 30 at.%, this metastable austenitic phase eventually transforms to a face-centered tetragonal (fct) martensitic phase if the temperature is lowered further. It is this transformation that is responsible for the shape memory effect in these alloys. At lower Pd contents, the austenite transforms to a body-centered tetragonal (bct) martensite. This transformation is not thermoelastic and does not produce any shape memory effect.[14–16]

In this study, we investigate the structure and thermomechanical behavior of Fe–Pd thin film. Fe–Pd coatings with a range of compositions have been prepared by

[a)]Address all correspondence to this author.
e-mail: vlassak@esag.harvard.edu
DOI: 10.1557/JMR.2005.0283

means of magnetron sputtering using a confocal sputter gun arrangement. The structure of both as-deposited and heat-treated films is analyzed using x-ray diffraction. The stress–temperature behavior of the films is explored using the substrate curvature technique.

II. EXPERIMENTAL DETAILS

Fe–Pd thin films of various compositions were grown by means of direct current (dc) magnetron sputtering. All depositions were performed in a model ATC 1800 sputter deposition system from AJA International equipped with three confocal sputter guns. The chamber configuration is illustrated schematically in Fig. 1. In previous studies,[10,12,13] films that were sputter deposited from Fe–Pd alloy targets, consistently showed a deficiency in the Pd content. To avoid this problem, the films in this study were grown using elemental Fe and Pd targets instead. By varying the power to individual sputter guns, films with a wide range of tailored compositions were obtained with just two targets. The base pressure of the deposition system was less than 1.7×10^{-7} Torr; the Ar working gas pressure was 5 mTorr for all runs. All films were grown at room temperature on (100) Si substrates coated with 200 nm of Si_3N_4 deposited using low-pressure chemical vapor deposition (LPCVD). Si substrates with a thickness of only 200 μm were used to improve the resolution of the film stress measurements. The purpose of the Si_3N_4 coating was to prevent the formation of silicides at the film/substrate interface during subsequent heat treatments. The inclination of the sputter guns was fixed at 21° and the working distance (WD) was maintained at approximately 100 mm for all depositions. During deposition, the substrates were rotated at a speed of 17 revolutions per minute for optimum film thickness and compositional uniformity. The power applied to the Fe and Pd targets (∅ 50.8 mm) was varied between 200 and 320 W and between 30 and 54 W, respectively. Film thickness and composition were analyzed with Rutherford back-scattering spectrometry (RBS) using a 1.7-MV General Ionex Tandetron Accelerator equipped with both a gas and a heavy-ion source. Film thicknesses varied between 0.6 and 1 μm. To obtain the metastable face-centered-cubic (fcc) phase at room temperature, as-deposited films were heat treated at 900 °C for 15 min followed by a quench in flowing Ar. All heat treatments were performed in an atmosphere of oxygen-gettered Ar inside a vacuum furnace with a base pressure of less than 5×10^{-6} Torr. This procedure has been shown to produce the fcc phase without excessive oxidation of the specimens.[11]

The crystal structure of both as-deposited and heat-treated films was analyzed by means of x-ray diffraction (XRD) using a Philips PW1010 diffractometer and Cu K_α radiation. The film surface morphology was observed using a LEO 982 scanning electron microscope (SEM). Heat-treated films were ferromagnetic as demonstrated by their interaction with a permanent magnet. The mechanical behavior of both as-deposited and heat-treated films was examined by measuring the film stress as a function of temperature using the substrate curvature technique. Specimens were thermally cycled between 15 and 200 °C in an Ar atmosphere while the curvature of the substrates was monitored using a scanning laser beam. Stoney's equation[17] was used to convert experimental curvatures into film stress. The stress in the Si_3N_4 coatings in both as-deposited state and after heat treatment was determined from separate samples without Fe–Pd films.

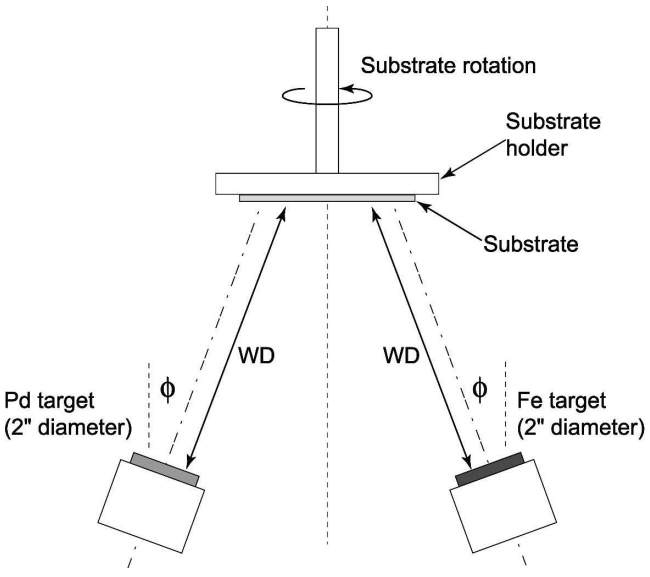

FIG. 1. Schematic illustration of the sputter chamber configuration.

III. EXPERIMENTAL RESULTS AND DISCUSSION

A. As-deposited films

Figure 2 shows the variation in Pd content of as-deposited films as a function of the power applied to the Pd target normalized with the total power applied to both targets. There is a linear increase in Pd content as the power to the Pd target is raised. The scatter in composition at a given power level is mainly due to changes in deposition rate that arise as the surface topography of the Fe target evolves. The permanent magnet configuration used for sputtering a ferromagnetic material such as Fe results in a narrow erosion pattern on the target. During the course of the Fe target life, the erosion pattern deepens into a groove and the deposition rate changes. The magnetic field used for sputtering Pd is weaker and target erosion is not nearly as severe. By tracking the Pd concentration over the lifetime of an Fe target, films of reproducible composition can be grown. Across a 100-mm substrate, compositional variation was typically less than

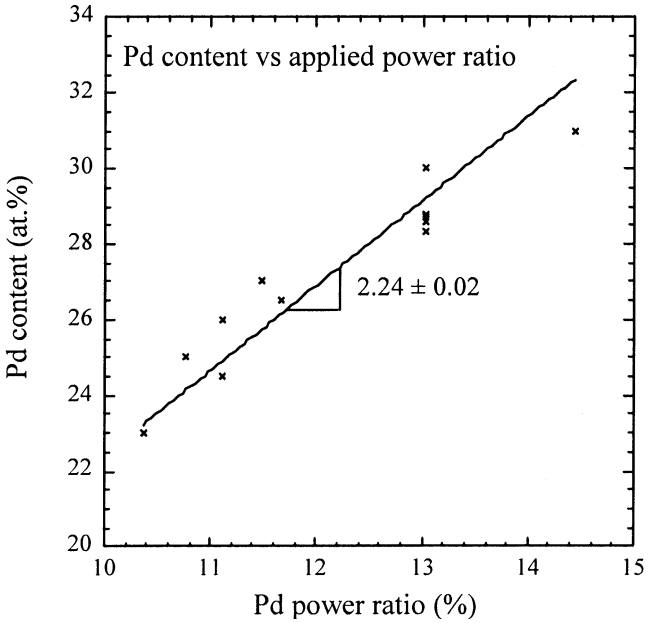

FIG. 2. Variation of Pd content in as-deposited Fe–Pd films with the ratio of the power applied to the Pd target to the total power applied to both targets.

0.5 at.%, while thickness uniformity was better than 2.5%.

Figure 3 shows SEM micrographs of the surface of a 0.6-μm Fe–Pd film containing 28.8 at.% Pd before and after heat treatment. The as-deposited film has a very fine structure with surface features in the range of 50–100 nm. A plan-view transmission electron microscope (TEM) investigation of the film reveals a grain size of approximately 50 nm, suggesting that the features in Fig. 3(a) correspond to individual grains in the film. The heat-treated film has a grain size on the order of 1–2 μm, which is somewhat larger than expected for a film of this thickness. There is a distinct formation of steps or ledges on the film surface. A similar surface morphology was observed recently by Inoue et al.[9] in heat-treated films containing fct martensite with a grain size of 2–4 μm. The x-ray diffraction spectra for as-deposited films with Pd content ranging from 26 to 30 at.% are depicted in Fig. 4. The films show a broad peak near 43° and a small sharp peak at 47.7°. The latter is due to diffraction by the Si substrate and can be ignored. The equilibrium phases for films in this composition range[18] are body-centered-cubic (bcc) Fe and the ordered Fe–Pd phase. These phases would result in diffraction peaks near 41°, 45°, 47°, and 49°, which are clearly not observed. Instead, the films consist of a supersaturated solid solution of Pd in bcc Fe that produces a (110) reflection at 43°. The structure of the films is further confirmed by the presence of (200) and (211) reflections at higher angles, not shown in Fig. 4, and by the corresponding electron diffraction rings in the TEM study. The (110) peaks in the diffraction spectra in Fig. 4 are quite broad as expected for films with a very

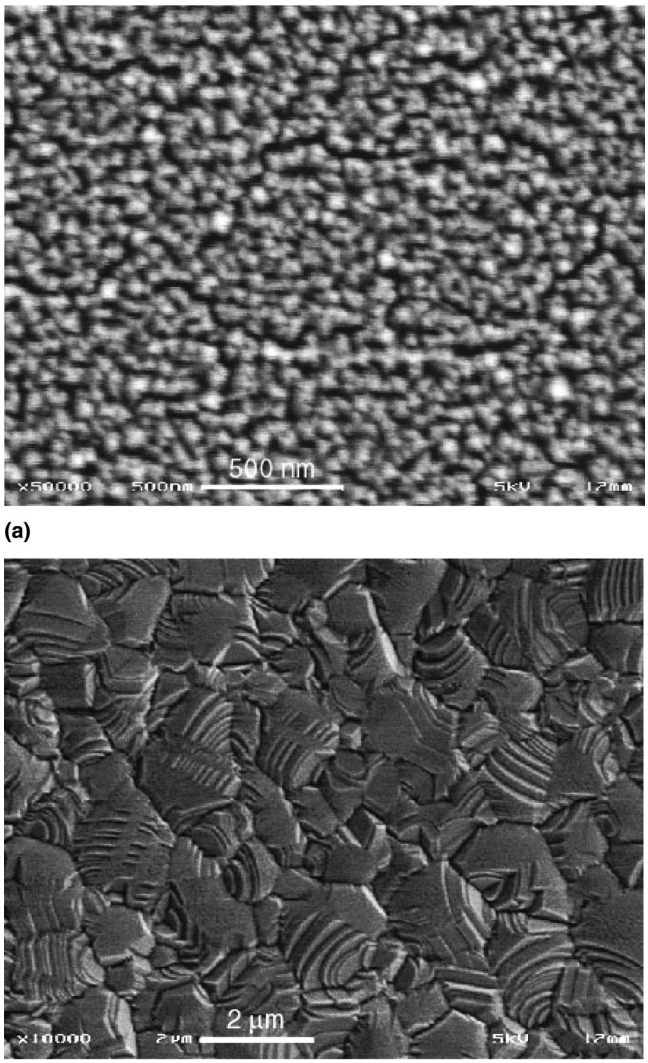

FIG. 3. SEM micrographs of a 0.6 μm film with 28.8 at.% Pd (a) before and (b) after heat treatment at 900 °C.

small grain size. If peak broadening is attributed solely to grain size and instrumental broadening, one obtains a lower-bound estimate for the grain size of approximately 10 nm, in good agreement with the TEM observations.

As-deposited films were subjected to a thermal cycle between room temperature and 200 °C to investigate their thermomechanical behavior. Figure 5 shows the residual stress in the films as a function of temperature during these cycles. For clarity, curves for different Pd concentrations have been offset; the precise room-temperature values of the residual stress can be found in Fig. 6. As the specimens are heated, the residual stress becomes more compressive, as one would expect for a metal film on a Si substrate. At a temperature of approximately 100 °C, the stress stops decreasing and remains more or less level with increasing temperature. On cooling from 200 °C, the stress decreases in a linear and

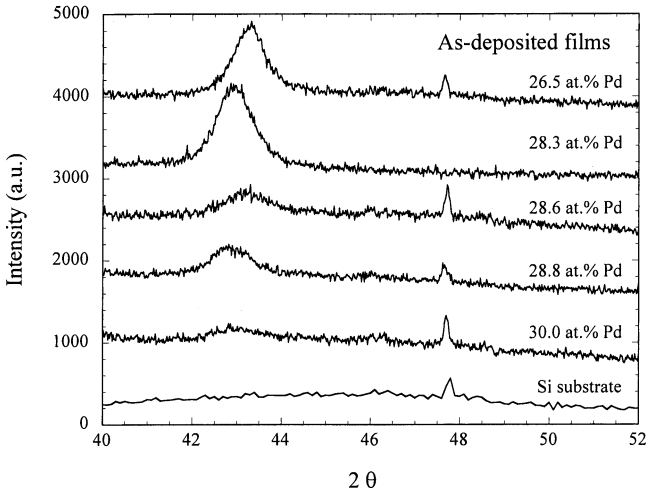

FIG. 4. XRD spectra for as-deposited films with Pd contents ranging from 26.5 to 30 at.%. Spectra have been offset for clarity.

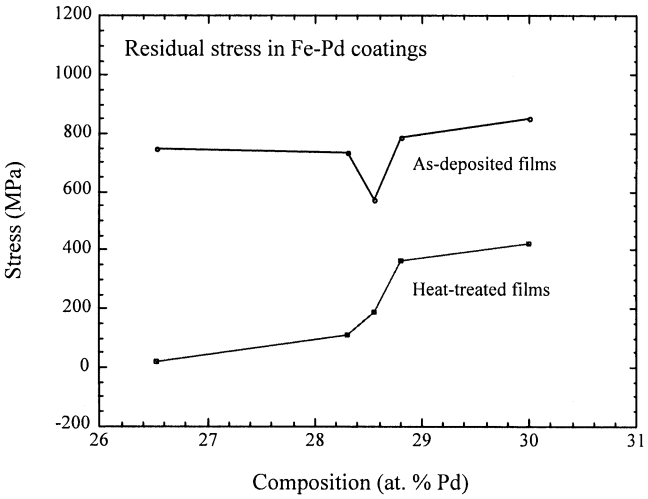

FIG. 6. Residual stress in as-deposited and heat-treated films with Pd contents ranging from 26.5 to 30 at.%.

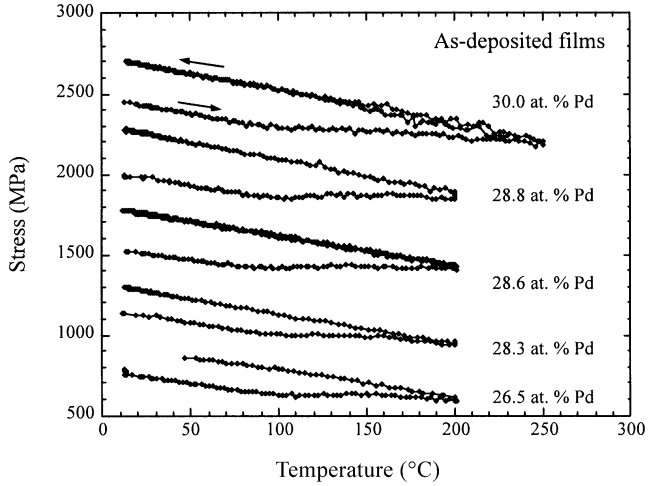

FIG. 5. Film stress in as-deposited specimens as a function of temperature during thermal cycles. Curves have been offset for clarity. Initial values of the residual stress are given in Fig. 6. The curves for films with 28.6% and 30.0% Pd consist of two thermal cycles.

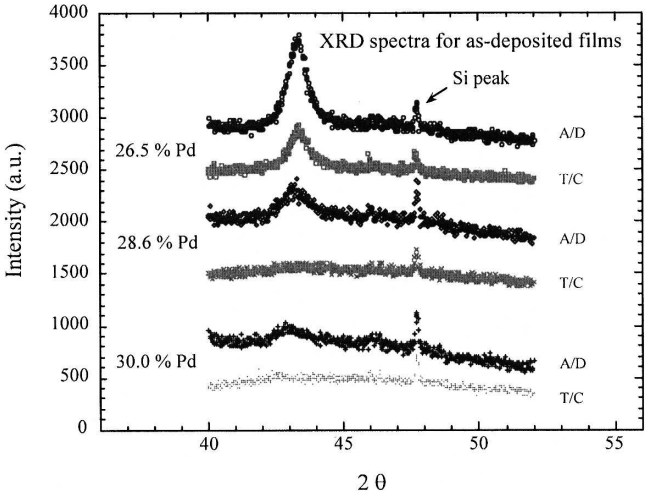

FIG. 7. XRD patterns for selected films before (A/D) and after (T/C) thermally cycling to 200 °C.

reversible fashion; additional temperature cycles trace the upper branch of the curve nearly perfectly. This reversibility suggests that the anomalous behavior on heating is exhausted by 200 °C. The behavior on heating is indicative of a densification of the film and is similar to the behavior observed for sputter-deposited Fe–Ni films.[19] The same densification is also observed in bulk Fe–Pd ingots that are annealed at 1150 °C and quenched from this temperature.[20] For compositions with 28 at.% Pd or less these ingots consist of a supersaturated solid solution of Pd in Fe with a bcc structure, similar to the coatings in this study. It has been suggested[19] that the densification in Fe–Ni coatings is due to grain growth. This does not seem to be the case here. Figure 7 shows the x-ray diffraction patterns for selected films before and after the thermal cycle. Rather than becoming narrower as one would expect in case of grain growth, the diffraction peaks are reduced in intensity or have disappeared altogether after the thermal cycle. Thus, it is more likely that the observed behavior is associated with a structural change in the film. Similar behavior is observed in highly supersaturated Nb–Co and Fe–W alloys prepared by co-sputtering of the constituents.[21–23] As deposited, these films have a bcc structure, which upon annealing decomposes into an amorphous phase and—depending on composition—another bcc phase. This behavior is observed in supersaturated alloys with a substantial atomic size difference between the constituents. The size mismatch destabilizes the crystalline solid solution and provides a driving force for the formation of an amorphous phase that can more easily tolerate large atomic size differences.[23] It is interesting to note that according to Fig. 5 this process leads to densification of

the films. As pointed out by Matsui and colleagues,[20] this may be the result of the formation of a small amount of an Fe-rich bcc phase, which is not as yet detected in the XRD spectra in Fig. 7.

Figure 8 shows how the change in residual stress during the thermal cycle varies with the Pd content of the film. There is an abrupt increase around 28 at.% Pd. It is interesting to note that this sudden rise coincides with the transition from the bcc to fcc structure in quenched bulk specimens.[20,25] In the coatings examined in this study, however, there is no evidence of the formation of the fcc phase in the as-deposited films. It should further be pointed out that the step in Fig. 8 is not due to a sudden rise in film stiffness as the Pd content of the films increases. Such a rise would require a corresponding change in the slope of the stress–temperature curves, since this slope is determined by the product of the biaxial elastic modulus of the film, M_f, and the difference in thermal expansion coefficients of substrate and film

$$\frac{d\sigma}{dT} = M_f(a_s - a_f) \quad . \tag{1}$$

A sudden change in the slope of the stress–temperature curves is not observed in Fig. 8, confirming that the step in Fig. 8 is indeed due to a rise in the degree of densification over this composition range.

Not much is known about the elastic properties of supersaturated Fe–Pd films with this type of microstructure. From the room-temperature single-crystal elastic constants for an alloy with 30% Pd,[24] the biaxial modulus for a film with a (110) fiber texture is estimated to be approximately 157 GPa. Using Eq. (1), this modulus results in an average coefficient of thermal expansion of $(1.5 \pm 0.1) \times 10^{-5}$ K^{-1}, which is close to the thermal expansion coefficient of both bulk Fe and Pd. The biaxial modulus for a random polycrystalline material yields nearly the same result.

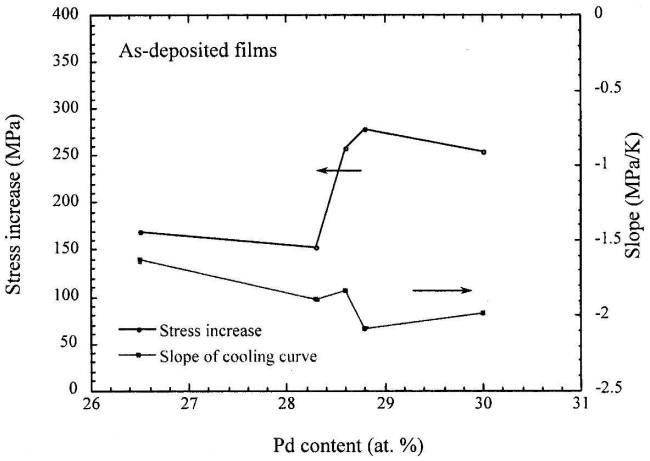

FIG. 8. Change in residual stress after one thermal cycle and slope of the cooling curves as a function of Pd content of the film.

B. Heat-treated films

Figure 9 shows XRD spectra for films after heat treatment. When the Pd content is high, the films consist of the fcc austenite phase only. As the Pd concentration decreases, the (200) reflection splits into two separate (200) and (002) peaks, indicating that the film has transformed to fct martensite.[26] This observation is confirmed by the broadening of the (311) peak at higher diffraction angles, not shown in the figure. A small peak corresponding to the (200) reflection of the fcc phase remains suggesting that that the martensitic transformation is incomplete. As expected, no splitting is observed for the (111) reflection. The film with 26.5% Pd consists mainly of a mixture of fcc and bct phases indicating that the transformation of fcc to bct is incomplete at room temperature. There is also a weak peak at 43.6°, which can be attributed to a small amount of bcc Fe formed during quenching.

Stress-temperature curves for heat-treated films are depicted in Fig. 10. Curves for films with different Pd

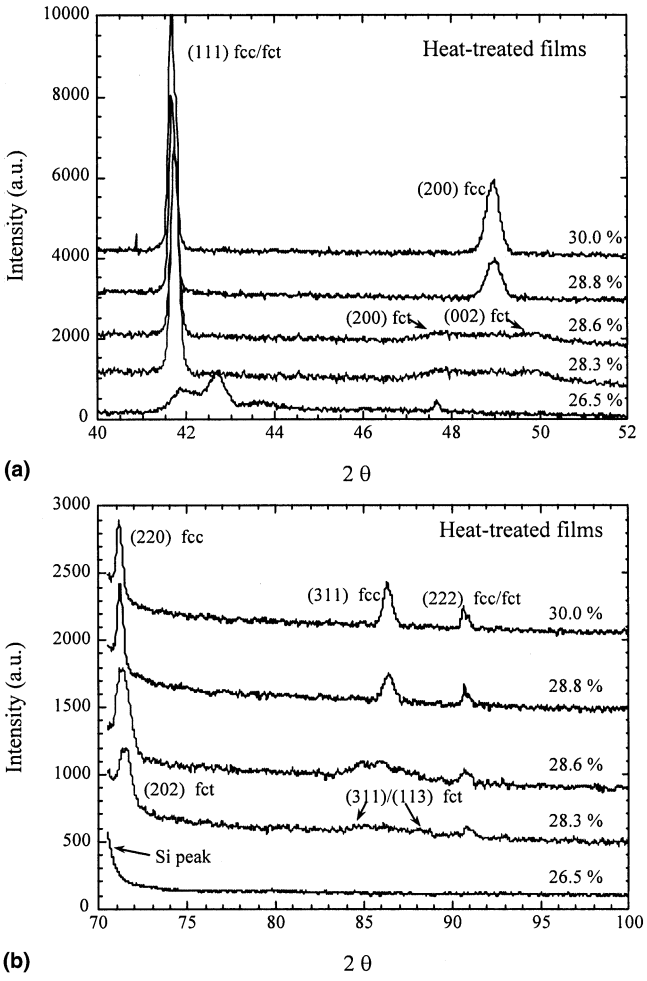

FIG. 9. XRD spectra for heat-treated films with Pd content ranging from 26.5 to 30 at.%: (a) low diffraction angles; (b) high diffraction angles.

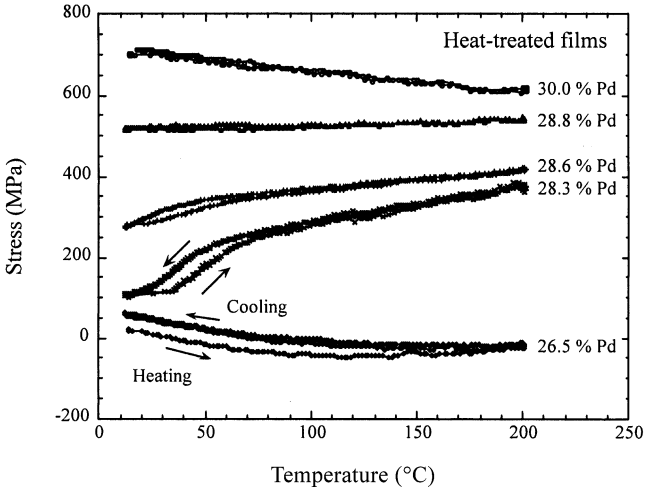

FIG. 10. Film stress in heat-treated specimens as a function of temperature during thermal cycles. Curves have been offset for clarity. The actual initial room-temperature values of the residual stress are given in Fig. 6. Curves for the three lowest Pd concentrations represent two thermal cycles.

content have been offset for clarity; the initial room-temperature values of the residual stress are given in Fig. 6. The stress–temperature behavior of the heat-treated specimens is remarkable in two respects: some of the curves show a fairly sudden and reversible stress change and the slope of the stress–temperature curves is a strong function of Pd content of the films.

The residual stress in the coating with 28.3% Pd rises abruptly when the temperature is increased above room temperature. This stress increase is associated with the transformation of the martensitic phase to the fcc austenite phase. The transformation is complete when the temperature exceeds 70 °C. On cooling, the austenite phase transforms back to martensite partially relaxing the stress in the film. During subsequent thermal cycling, the stress versus temperature curve follows that of the first thermal cycle, validating the thermoelastic nature of the fcc to fct transformation in these films. Transformation to martensite results in a lowering of the stress in the films since those martensitic variants will be formed during the transformation that best accommodate the strain in the film. The total temperature hysteresis is only about 15 °C. When the Pd content is increased to 28.6% Pd, the transformation takes place at lower temperature, in agreement with results for bulk materials.[14–16] From the shape of the stress–temperature curve, it is apparent that the transformation in this specimen is not yet complete at room temperature. This observation is confirmed by the diffraction results in Fig. 9, which indeed show a weak (200) reflection for the austenite phase. If the Pd content is increased further, the transformation temperature decreases below room temperature and no stress drop is discerned in the stress–temperature curves. At lower Pd concentrations, the film transforms to bct martensite on quenching. This martensitic transformation is not reversible.[14] Consequently, there are no abrupt stress changes as the temperature of the film is cycled.

In bulk Fe–Pd alloys, the fct martensitic transformation is known to occur well below room temperature in a narrow composition range around 30 at.% Pd. As shown by the diffraction results and the film stress measurements, the temperature range over which the fct martensite exists in thin films can be raised above room temperature. This experimental observation of increased transformation temperature in the presence of a tensile stress is consistent with the Clausius–Clapeyron equation[27] and has also been observed for other shape memory alloy thin films.[28,29] The trend is consistent with experimental results obtained by Kato et al.,[30] demonstrating that stress-induced fct martensite can be obtained near room temperature in bulk polycrystalline Fe–Pd samples. Their results suggest that the transformation temperature in unstressed films would be approximately 50 °C lower than the temperatures measured in this study. It should further be noted that the transformations take place at lower Pd concentrations than reported for bulk materials. Formation of bct martensite is reported at 29.5% Pd in bulk materials,[15,16] while fct martensite is observed at concentrations as low as 28.3% in the current study. This observation is also confirmed by x-ray diffraction results obtained for thin Fe–Pd films by Inoue et al.[9] The capability of stabilizing fct martensite near room temperature over a wider range of compositions than in bulk materials makes Fe–Pd shape-memory thin films more attractive for practical applications.

A second observation worthy of note with respect to Fig. 10 is the strong dependence of the slopes of the stress–temperature curves on the Pd content of the films. As mentioned earlier, metallic films deposited on Si substrates typically exhibit a decrease in residual stress with increasing temperature. This follows directly from Eq. (1) and the observation that the thermal expansion coefficients of most metallic materials are several times larger than that of Si. From that point of view, the stress–temperature curves of the as-deposited films in Fig. 5 are typical for metallic films. The behavior of the heat-treated films in Fig. 10, however, is unusual. Films with a composition of 28.3% Pd or more show an *increase* in stress in the temperature range where the fcc austenite phase is stable. The same trend is also observed for the temperature range where the fct phase is stable in the specimen with 28.3% Pd. The sample with the bct structure, by contrast, shows a decrease in stress with increasing temperature. Furthermore, the behavior is fully reversible with several heating cycles resulting in virtually identical curves. This, of course, excludes densification as a possible mechanism. The anomalous behavior can be attributed to the existence of very low values of the coefficient of thermal expansion in Fe–Pd alloys containing

approximately 30 at.% Pd, i.e., the Invar effect. This phenomenon was first observed in Fe–Ni alloys by Guillaume well over 100 years ago, and was subsequently demonstrated in bulk Fe–Pt and Fe–Pd alloys.[31] The thermal expansion coefficients obtained from the data in Fig. 10 are plotted as a function of Pd content in Fig. 11. The thermal expansion coefficients in this figure were calculated from Eq. (1) using a thermal expansion coefficient of Si of 2.8×10^{-6}/°C and the biaxial elastic modulus of an Fe–Pd film with a (111) fiber texture. This modulus was determined from the single-crystal elastic constants for a magnetically saturated fcc alloy with 30% Pd[24] and is equal to 254 GPa. Figure 11 clearly demonstrates that the coefficient of thermal expansion of the films is indeed much smaller than one would expect for typical metals and that in one case it is even negative. It should be noted that the modulus used to derive these results is an upper bound and that the actual modulus may be somewhat lower. A lower modulus would decrease the numerical values of the thermal expansion coefficient even further. Compared to measurements for bulk Fe–Pd alloys, the thermal expansion coefficients are smaller and occur at lower temperatures and Pd contents.[20,32] The minimum value measured for a bulk Fe–Pd alloy with 32% Pd, for instance, is approximately 2×10^{-6}/°C and occurs near 550 K; the room-temperature value for the same alloy is 9×10^{-6}/°C.[32] One factor that needs to be considered when analyzing this difference is the effect of the temperature dependence of the elastic constants, which can be quite large for materials that show martensitic transformations. The thermal expansion coefficients in Fig. 11 were calculated assuming that the elastic constants do not vary with temperature. If that is not the case, an additional term appears in Eq. (1)

$$\frac{d\sigma}{dT} = M_f(a_s - a_f) + \frac{\sigma}{M_f}\frac{dM_f}{dT} \quad . \tag{2}$$

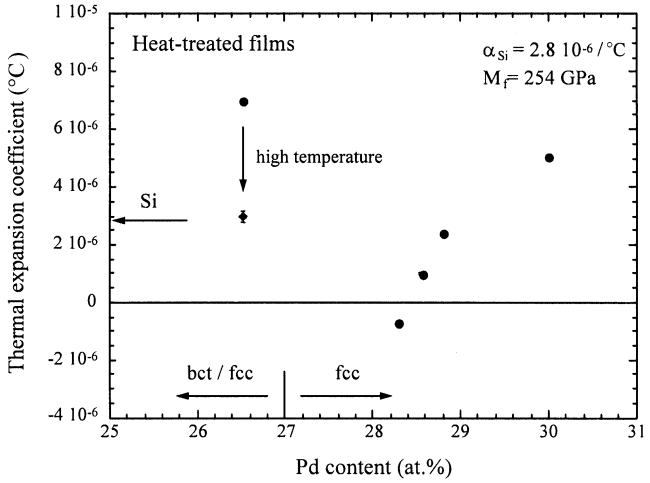

FIG. 11. Thermal expansion coefficients as a function of Pd content of the film. Error bars are smaller than data points in most cases.

The last term in the right-hand side of this equation depends on the temperature coefficient of the biaxial elastic modulus. Because most materials become more compliant with increasing temperature, including this term in the calculation normally lowers the value of the thermal expansion coefficient. In this case, the effect is not immediately obvious because an increase in temperature also results in an increase in stress in most films. This in turn leads to a higher modulus through a reduction of the ΔE effect and hence a positive apparent temperature coefficient for the elastic modulus. Consequently, the modulus correction could either lower or increase the thermal expansion coefficient depending on the relative magnitude of both effects. An estimate of the order of magnitude of the correction can be obtained as follows. Films with a (111) fiber texture that contain 30% Pd have a negative temperature coefficient for the biaxial modulus (approximately –0.13 GPa/K) contrary to most other elastic constants of this alloy[24] and a ΔE effect of 8%.[33] The correction to the thermal expansion coefficient due to the temperature coefficient of the elastic modulus is then -6×10^{-7} K^{-1}. If one assumes that the entire ΔE effect is exercised over one thermal cycle in Fig. 10, then one obtains an upper bound for the ΔE correction of approximately 9×10^{-7} K^{-1}. From this discussion, it is clear that the temperature dependence of the modulus alone cannot explain the difference in thermal expansion behavior between films and bulk material. The thermal expansion of Invar alloys, however, is known to depend on their microstructure and thermomechanical history.[34] The origin of the low thermal expansion coefficients of the films may well lie in their fine microstructure [e.g., Fig. 3(b)] and the high stresses supported by them.

The Invar effect is known to occur in the fcc phase close to the fcc–bcc phase boundary.[35] Because the fct/bct phase boundary is shifted to lower Pd contents in thin films compared to the bulk, one might reasonably expect a similar shift for the Invar effect. The stress–temperature results in Fig. 10 indicate that the fct phase also shows the Invar effect, even though measurements are limited to a small temperature range. Clearly, the tetragonality of the crystal structure is not sufficient to destroy the effect. The behavior of the film with 26.5% Pd deserves some consideration as well. At low temperature, the stress decreases with increasing temperature, as one would expect for a metal film on a Si substrate. When the temperature exceeds 80 °C, however, the stress levels off and remains unchanged with increasing temperature. This behavior is similar to that of the as-deposited films except that now the effect is reversible: with the exception of the first heating curve, all curves overlap perfectly. This rules out a phase transformation or irreversible densification of the film. The behavior can be understood, however, if one realizes that the film consists of a mixture of the bct and

fcc phases as indicated by the diffraction results. The bcc phase has a normal thermal expansion coefficient. If the fcc phase shows the Invar effect for temperatures above 80 °C, the thermal expansion of the film is reduced in this temperature range. The corresponding thermal expansion coefficient is shown in Fig. 11.

IV. CONCLUSIONS

Fe–Pd thin films with a range of compositions were deposited by means of magnetron sputtering of elemental Fe and Pd targets. As-deposited films are highly supersaturated solid solutions with a bcc crystal structure and a very fine grain structure. These films have thermal expansion coefficients that are typical for metallic films. On heating the films in the 100–200 °C range, they undergo a structural change similar to that observed in other supersaturated systems with a substantial atomic size difference between the constituents. This change leads to the formation of an amorphous phase and possibly an Fe-rich bcc phase.

The austenite, which is the stable high-temperature phase, can be retained at a much lower temperature by a post-deposition heat treatment that consists of an anneal at 900 °C followed by rapid cooling in flowing Ar. As the temperature is lowered, this phase undergoes a martensitic transformation that results in either a bct or an fct martensite, depending on composition. The fct martensite occurs in a narrow composition range at 28 at.% Pd, while the bct martensite is formed at lower Pd contents. The formation of fct martensite is reversible and results in a significant drop of the residual stress in the film. This stress drop is recovered as the films transform back to austenite on heating. The bct martensitic transformation is not reversible. It should be noted that the fct martensitic transformation occurs both at lower Pd contents and at higher temperatures than reported for bulk materials making Fe–Pd in thin film form more attractive for practical application.

Heat-treated films with either the fct or fcc crystal structure show the Invar effect, i.e., they have very low coefficients of thermal expansion compared to typical metal films. The coefficients of thermal expansion found in this study are significantly smaller than the corresponding values for bulk Fe–Pd alloys. Moreover, the Invar effect occurs at lower temperatures and Pd contents than reported for bulk materials. This shift seems to correlate with the shift in the fct–bct phase boundary observed in these films.

ACKNOWLEDGMENTS

This work was funded by a Seed Money grant from the Center for Imaging and Mesoscale Structures at Harvard University. T.C.-K. was supported by the Research Experience for Undergraduates program funded by the National Science Foundation (DMR-0213805). The authors thank Frans Spaepen for use of the substrate curvature system, T.Y. Tsui for supplying the Si_3N_4-coated substrates, and Xi Wang for the TEM work.

REFERENCES

1. K. Shimizu and T. Kakeshita: Effect of magnetic fields on martensitic transformations in ferrous alloys and steels. *ISIJ Int.* **29,** 97 (1989).
2. D.P. Dunne and C.M. Wayman: The effect of austenite ordering on the martensite transformation in Fe-Pt alloys near the composition Fe_3Pt: I. Morphology and transformation characteristics. *Metall. Trans.* **4,** 137 (1973).
3. D.P. Dunne and C.M. Wayman: The effect of austenite ordering on the martensite transformation in Fe-Pt alloys near the composition Fe_3Pt: II. Crystallography and general features. *Metall. Trans.* **4,** 147 (1973).
4. R.D. James and M. Wuttig: Magnetostriction of martensite. *Philos. Mag. A* **77,** 1273 (1998).
5. T. Kakeshita, T. Takeuchi, T. Fukuda, M. Tsujiguchi, T. Saburi, R. Oshima, and S. Muto: Giant magnetostriction in an ordered Fe_3Pt single crystal exhibiting a martensitic transformation. *Appl. Phys. Lett.* **77,** 1502 (2000).
6. H. Kato, T. Wada, Y. Liang, T. Tagawa, M. Taya, and T. Mori: Martensite structure in polycrystalline Fe–Pd. *Mater. Sci. Eng.* **A332,** 134 (2002).
7. R.C. O'Handley: Model for strain and magnetization in magnetic shape memory alloys. *J. Appl. Phys.* **83,** 3263 (1998).
8. K. Ullakko, J.K. Huang, C. Kantner, R.C. O'Handley, and V.V. Kokorin: Large magnetic-field-induced strains in Ni_2MnGa single crystals. *Appl. Phys. Lett.* **69,** 1966 (1996).
9. S. Inoue, K. Inoue, S. Fujita, and K. Koterazawa: Fe–Pd ferromagnetic shape memory alloy thin films made by dual source DC magnetron sputtering. *Mater. Trans.* **44,** 298 (2003).
10. S. Inoue, K. Inoue, K. Koterazawa, and K. Mizuuchi: Shape memory behavior of Fe–Pd alloy thin films prepared by dc magnetron sputtering. *Mater. Sci. Eng.* **A339,** 29 (2003).
11. Y. Sugimura, T. Cohen-Karni, P. McCluskey, and J.J. Vlassak: Fabrication and characterization of Fe–Pd ferromagnetic shape-memory thin films, in *Materials and Devices for Smart Systems*, edited by Y. Furuya, E. Quandt, Q. Zhang, K. Inoue, and M. Shahinpoor (Mater. Res. Soc. Symp. Proc. **785,** Warrendale, PA, 2004), D7.4.1, p. 201.
12. Z. Wang, T. Iijima, G. He, K. Oikawa, L. Wulff, N. Sanada, and Y. Furuya: Preparation of sputter-deposited Fe–Pd thin films. *Mater. Trans., Jpn. Inst. Met.* **41,** 1139 (2000).
13. Z. Wang, T. Iijima, G. He, T. Takahashi, and Y. Furuya: Structural characteristics and magnetic properties of Fe–Pd thin films. *Int. J. Appl. Electromag. Mech.* **12,** 61 (2000).
14. R. Oshima: Successive martensitic transformations in Fe–Pd alloys. *Scripta Metall.* **15,** 829 (1981).
15. M. Sugiyama, R. Oshima, and F.E. Fujita: Martensitic transformation in the Fe–Pd alloy system. *Trans. Jpn. Inst. Met.* **25,** 585 (1984).
16. M. Sugiyama, R. Oshima, and F.E. Fujita: Mechanism of fcc–fct thermoelastic martensite transformation in Fe–Pd alloys. *Trans. Jpn. Inst. Met.* **27,** 719 (1986).
17. M.F. Doerner and W.D. Nix: Stresses and deformation processes in thin films on substrates. *CRC Crit. Rev. Solid State Mater. Sci.* **14,** 225 (1988).
18. P. Villars and L.D. Calvert: *Pearson's Handbook of Crystallographic Data for Intermetallic Phases* (American Society for Metals, Metals Park, OH, 1985).

19. R-M. Keller-Flaig and E. Arzt: Mechanical and thermal expansion behavior of thin Fe-36 wt.-% Ni Invar films. *Adv. Eng. Mater.* **4,** 305 (2002).
20. M. Matsui, T. Shimizu, and K. Adachi: Invar anomalies of Fe–Pd alloys. *Physica* **119B,** 84 (1983).
21. H.Y. Bai, C. Michaelsen, and R. Bormann: Inverse melting in a system with positive heats of formation. *Phys. Rev. B* **56,** R11 (1997).
22. W. Biegel, W. Schaper, H-U. Krebs, J. Hoffmann, H.C. Freyhardt, R. Busch, and R. Bormann: Phase-transformations of supersaturated sputtered Nb Co films. *J. Phys.* **51,** C4189 (1990).
23. R. Bormann: Thermodynamic and kinetic requirements for inverse melting. *Mater. Sci. Eng. A* **179/180,** 31 (1994).
24. S. Muto, R. Oshima, and F.E. Fujita: Elastic softening and elastic strain-energy consideration in the fcc–fct transformation of Fe–Pd alloys. *Acta Metall. Mater.* **38,** 685 (1990).
25. R. Oshima, S. Muto, and F.E. Fujita: Initiation of fcc–fct thermoelastic martensite-transformation from premartensitic state of Fe-30 at percent-Pd alloys. *Mater. Trans. Jpn. Inst. Met.* **33,** 197 (1992).
26. T. Sohmura, R. Oshima, and F.E. Fujita: Thermoelastic fcc-fct martensitic transformation in Fe–Pd alloy. *Scripta Metall.* **14,** 855 (1980).
27. P. Wollants, J.R. Roos, and L. Delaey: Thermally-induced and stress-induced thermoelastic martensitic transformations in the reference frame of equilibrium thermodynamics. *Prog. Mater. Sci.* **37,** 227 (1993).
28. S. Miyazaki and A. Ishida: Shape memory characteristics of sputter-deposited Ti–Ni thin films. *Mater. Trans. Jpn. Inst. Met.* **35,** 14 (1994).
29. Y. Liu and X. Huang: Substrate-induced stress and transformation characteristics of a deposited Ti–Ni–Cu thin film. *Philos. Mag.* **84,** 1919 (2004).
30. H. Kato, Y. Liang, and M. Taya: Stress-induced fcc/fct phase transformation in Fe–Pd alloy. *Scripta Mater.* **46,** 471 (2002).
31. A. Kussmann and K. Jessen: Magnetische und dilatometrische Messungen zur Umwandlungskinetik der Eisen–Palladium Legierungen. *Z. Metallkd.* **54,** 504 (1963).
32. M. Matsui and K. Adachi: Magneto-elastic properties and Invar anomaly of Fe–Pd alloys. *Phys. B* **161,** 53 (1989).
33. T. Nakayama, M. Kikuchi, and K. Fukamichi: Young's modulus and the ΔE effect of Fe–Pd Invar alloys. *J. Phys. F: Metal Phys.* **10,** 715 (1980).
34. G. Hausch and P. Schrey: Thermal expansion of Invar and Superinvar after thermomechanical treatment. *Z. Metallkd.* **82,** 891 (1991).
35. M. Shiga: Invar alloys, in *Materials Science and Technology: A Comprehensive Treatment*, edited by R.W. Cahn, P. Haasen, and E.J. Kramer (VCH Verlagsgesellschaft GmbH, New York, 1990), pp. 159–210.